

Introducing 32 nm technology in Microwind35

Etienne SICARD

Professor

INSA-Dgei, 135 Av de Rangueil

31077 Toulouse – France

www.microwind.org

email: Etienne.sicard@insa-toulouse.fr

Syed Mahfuzul Aziz

School of Electrical & Information Engineering

University of South Australia

Mawson Lakes, SA 5095, Australia

www.unisa.edu.au

email: mahfuz.aziz@unisa.edu.au

This paper describes the improvements related to the CMOS 32 nm technology and the implementation of this technology in Microwind35. The main novelties related to the 32 nm technology such as the high-k gate oxide, 3rd generation channel strain, metal-gate and very low-K interconnect dielectric is described. The performances of a ring oscillator layout and a 6-transistor RAM memory layout are also analyzed.

1. Recent trends in CMOS technology

Firstly, we give an overview of the evolution of important parameters such as the integrated circuit (IC) complexity, gate length, switching delay and supply voltage with a prospective vision down to the 11 nm CMOS technology. The naming of the technology nodes (130, 90.. 11nm) comes from the International Technology Roadmap for Semiconductors [ITRS2009]. The trend of CMOS technology improvement continues to be driven by the need to

- Integrate more functions within a given silicon area
- Reduce the fabrication cost.
- Increase operating speed
- Dissipate less power

Table 1 gives an overview of the key parameters for technological nodes from 130 nm, introduced in 2001, down to 11 nm, which is supposed to be in production in the 2015-2018 timeframe. Demonstration chips using 32-nm technology have been reported by Intel in 2008 [Natarajan2008], and IBM in 2008 [Chen2008].

| Technology node | 130 nm | 90 nm | 65 nm | 45 nm | 32 nm | 22 nm | 16 nm | 11 nm |
|---|------------------|------------------|-------|--------|--------|--------|--------|---------|
| First production | 2001 | 2003 | 2005 | 2007 | 2009 | 2011 | 2013 | 2015 |
| Effective gate length | 70 nm | 50 nm | 35 nm | 30 nm | 25 nm | 18 nm | 12 nm | 9 nm |
| Gate material | Poly | Poly | Poly | Metal | Metal | Metal | Dual? | Triple? |
| Gate dielectric | SiO ₂ | SiO ₂ | SiON | High K |
| Raw M _{gates} /mm ² | 0.25 | 0.4 | 0.8 | 1.5 | 2.8 | 5.2 | 9.0 | 16.0 |
| Memory point (μ ²) | 2.4 | 1.3 | 0.6 | 0.3 | 0.17 | 0.10 | 0.06 | 0.06 |

Table 1: Technological evolution and forecast up to 2015

ARM, CHARTERED, IBM, SAMSUNG, and SYNOPSIS have agreement to develop a 32-nm technology enablement solution for the design and manufacture of mobile Internet-optimized devices [Common2009]. Mass market manufacturing with this technology is scheduled for 2011.

The gate material has long been polysilicon, with silicon dioxide (SiO₂) as the insulator between the gate and the channel (Fig. 1). The atom is a convenient measuring stick for this insulating material beneath the gate, commonly known as gate oxide. In the 90 nm technology, the gate oxide was consisting of about five atomic layers, equivalent to 1.2 nm in thickness. The thinner the gate oxide, the higher the transistor current

and consequently the switching speed. However, thinner gate oxide also means more leakage current. Starting with the 90nm technology, SiO₂ has been replaced by SiON dielectric, which features a higher permittivity and consequently improves the device performance while keeping the parasitic leakage current within reasonable limits.

Starting with the 45-nm technology, leakage reduction has been achieved through the use of various high-K dielectrics such as Hafnium Oxide HfO₂ ($\epsilon_r=12$), Zirconium Oxide ZrO₂ ($\epsilon_r=20$), Tantalum Oxide Ta₂O₅ ($\epsilon_r=25$) or Titanium Oxide TiO₂ ($\epsilon_r=40$). This provides much higher device performance as if the device was fabricated in a technology using conventional SiO₂ with much reduced “equivalent SiO₂ thickness”.

The High-K dielectric enabled a thinner “equivalent” oxide thickness (EOT) while keeping leakage current low. The “equivalent oxide thickness” EOT is defined by Equ. 1. For the 32-nm technology, the high-K permittivity declared in the rule file is 10 (Parameter “GateK”). The physical oxide thickness is 2.5 nm, and by applying Equ. 1, EOT is 1.0 nm. These parameters are in close agreement with those given by [Chen2008] (1.2nm) and [Natarajan2008] (0.9nm).

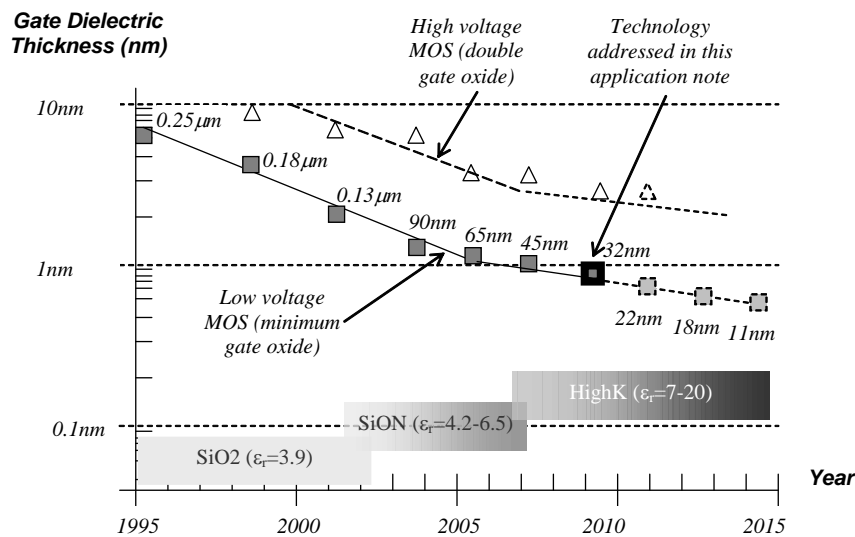


Figure 1 : The technology scale down towards nano-scale devices

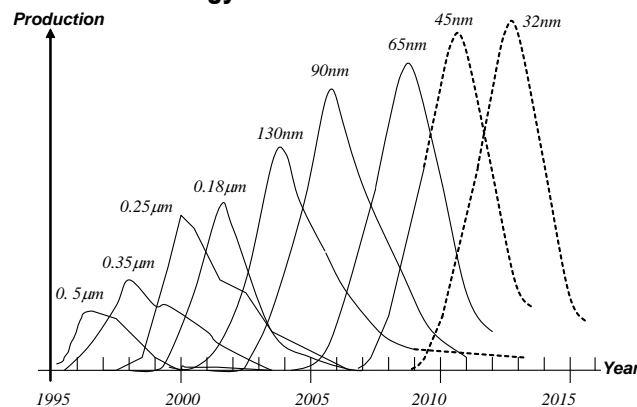


Figure 2 : Technology ramping every two years introducing the 32 nm technology

$$EOT = \left(\frac{\epsilon_{SiO_2}}{\epsilon_{high-k}} t_{high-k} \right) \quad (\text{Equ. 1})$$

Where

ϵ_{SiO_2} = dielectric permittivity of SiO₂ (3.9, no unit)

ϵ_{high-k} = High-K dielectric permittivity

t_{high-k} = High-K oxide thickness (m)

In the 32-nm technology node, most IC manufacturers use so called “HK-MG” gate stack, meaning a combination of high-K dielectric and metal gate. IBM 32nm use Hafnium Oxide to obtain an EOT close to 1.0 nm, and Intel claims an EOT of 0.9 nm (9 Å).

At each lithography scaling, the linear dimensions are approximately reduced by a factor of 0.7, and the area is reduced by factor of 2. Smaller cell sizes lead to higher integration density which has risen to nearly 2.8 million gates per mm² in the 32-nm technology.

The integrated circuit market has been growing steadily for many years, due to ever-increasing demand for electronic devices. The production of integrated circuits for various technologies over the years is illustrated in Fig. 2. It can be seen that a new technology has appeared regularly every two years, with a ramp up close to three years. The production peak is constantly increased, and similar trends should be observed for novel technologies such as 32-nm (forecast peak in 2013).

2. Transistor performances in 32-nm technology

Key features

Several 32-nm processes have been introduced by various manufacturers [Arnaud2008], [Chen2008], [Diaz 2008], [Hasegawa2008], [Natarajan2008], addressing different types of applications: IBM 32-nm technology is addressing low power applications such as mobile communication devices [Chen2008] while Intel is targeting high-performance microprocessors [Natarajan2008].

| Parameter | Value |
|-----------------------------------|-------------------------|
| V _{DD} (V) | 0.8-1.1 V |
| Effective gate length (nm) | 25-35 |
| Ion N (μA/μm) at 1V | 1000-1550 |
| Ion P (μA/μm) at 1V | 500-1210 |
| Ioff N (nA/μm) | 0.1-200 |
| Ioff P (nA/μm) | 0.1-100 |
| Gate dielectric | HfO ₂ , SiON |
| Equivalent oxide thickness (nm) | 0.9-1.2 |
| # of metal layers | 6-11 |
| Interconnect layer permittivity K | 2.4-3.0 |

Table 2: Key features of the 32 nm technology

Depending on the manufacturer, the transistor channels range from 25 nm to 35 nm in length (25 to 35 billionths of a meter). Some of the key features of the 32-nm technologies from various providers are given in Table 2. Compared to 45-nm technology, most 32-nm technologies offer:

- 30 % increase in switching performance
- 30 % less power consumption
- 2 times higher density
- X 2 reduction of the leakage between source and drain and through the gate oxide

Gate Material

For 40 years, the SiO₂ gate oxide combined with polysilicon have been serving as the key enabling materials for scaling MOS devices down to the 90 nm technology node. The gate dielectric thickness has been continually reduced to match the continuous requirements for improved switching performance, but the leakage current between drain/source and the gate became prohibitive. Consequently the oxide which has replaced SiO₂ is HfO₂ or HfSiON (Hafnium dielectric and silicate), featuring K between 16 and 24. Dielectrics with even higher permittivity (TiO₂, K near 80) are not used, as such materials induce severe parasitic electron tunneling [Skotnicki2008]. The optimum combination of high dielectric materials with metal gate materials features outstanding current switching capabilities together with low leakage. Increased *on* current, decreased *off* current and significantly decreased gate leakage are obtained with this novel combination.

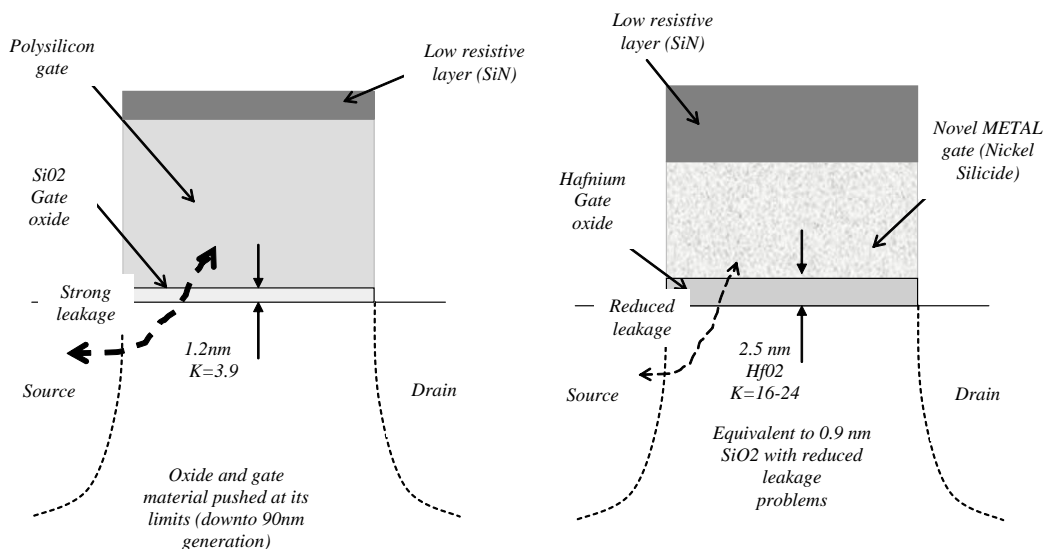


Figure 3: The metal gate combined with High-K oxide material enhances the MOS device performance in terms of switching speed and significantly reduces the leakage

Strained Silicon

Strained silicon has been introduced starting with the 90-nm technology [Sicard2006], [Sicard2007] to boost carrier mobility, which enhances both the n-channel and p-channel transistor performances. Figures 4 and 5 illustrate the strained silicon principles for NMOS and PMOS transistors respectively. PMOS transistor channel strain has been enhanced by increasing the Germanium (Ge) content in the compressive SiGe (silicium-germanium) film. Both transistors employ ultra shallow source-drains to further increase the drive currents.

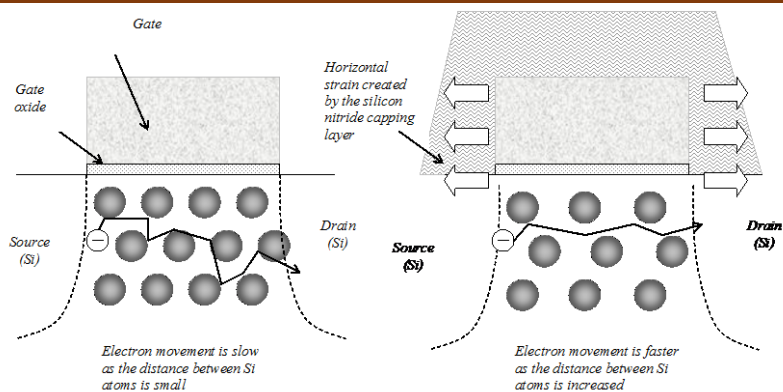


Figure 4: Tensile strain generated by a silicon-nitride capping layer increases the distance between atoms underneath the gate, which speeds up the electron mobility of n-channel MOS devices

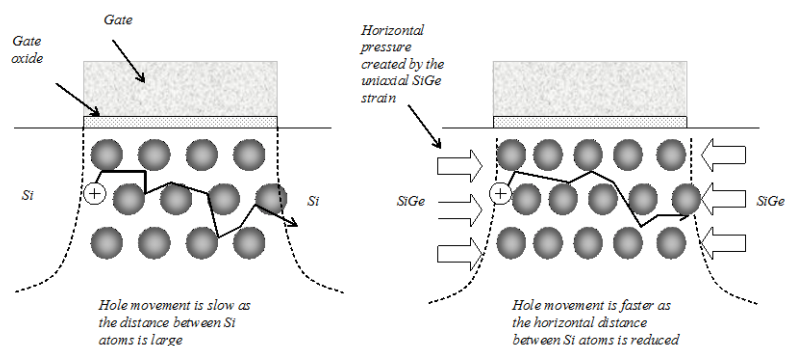


Figure 5: Compressive strain to reduce the distance between atoms underneath the gate, which speeds up the hole mobility of p-channel MOS devices

Let us assume that the silicon atoms form a regular lattice structure, inside which the carriers participating to the device current have to flow. In the case of electron carriers (NMOS), stretching the lattice (by applying tensile strain) allows the electrons to flow faster from the source to the drain, as depicted in Fig. 4. The mobility improvement exhibits a linear dependence on the tensile film thickness. In a similar way, compressing the lattice slightly speeds up the p-transistor, for which current carriers consist of holes (Fig. 5).

Intel has introduced a so-called “Replacement Metal Gate” (RMG) process flow in its 32 nm technology node [Natarajan2008] to further increase the channel strain, which consists of forming the Poly-Si gate first (Fig. 6a), then removing the gate (Fig. 6b) and then fabricating the Metal gate (Fig. 6c). The combination of reduced channel length, decreased oxide thickness and enhanced channel strain achieves a substantial gain in drive current for both nMOS and pMOS devices.

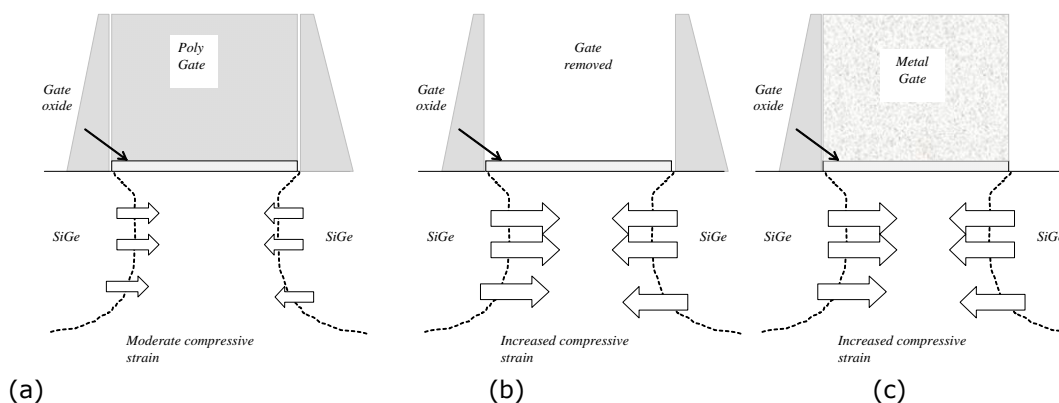


Figure 6: Increased p-channel MOS strain using a sacrificed poly gate and replacing it by metal gate [Natarajan2008]

MOS types

Some 32-nm technologies comprise as much as 10 types of MOS devices (i.e. 20 devices in total). In Microwind, only three types of MOS devices (3 nMOS, 3 pMOS, 6 MOS devices in total) exist in the 32-nm technology :

- ▶ the low-leakage MOS is the default MOS device,
- ▶ the high-speed MOS has higher switching performance, thanks to a shorter effective channel length, at the price of a much higher leakage.
- ▶ the high voltage MOS used for input/output interfacing. In Microwind's cmos32nm rule file, the I/O supply is 1.8 V. Some foundries also propose 2.5 V and 3.3 V interfacing.

The main objective of the low leakage MOS is to reduce the I_{off} current significantly, that is the small current that flows between drain and source with a zero gate voltage (See Table 3). The price to pay is a reduced I_{on} current. The designer has the choice of using high-speed MOS devices, which have high I_{off} leakages but large I_{on} drive currents. More details are provided in the following chapters.

N-channel MOS device characteristics

Microwind version 3.5 is configured by default to the 32-nm technology. This technology uses a stack of high-k dielectric and metal gate (TiN). Layouts and cross-sections of two varieties of n-channel MOS devices are given in Fig. 7 and 8, where the high-speed device has a reduced channel length (26 nm instead of 32 nm). Although the high speed NMOS has a slightly shorter channel, it is drawn with exactly the same size as the low leakage NMOS. The nMOS gate is capped with a specific silicon nitride layer that induces lateral tensile channel strain to improve electron mobility. The pMOS strain is based on SiGe diffusion and Replacement Metal Gate (RMG). Key parameters for the MOS devices are shown in Table 3.

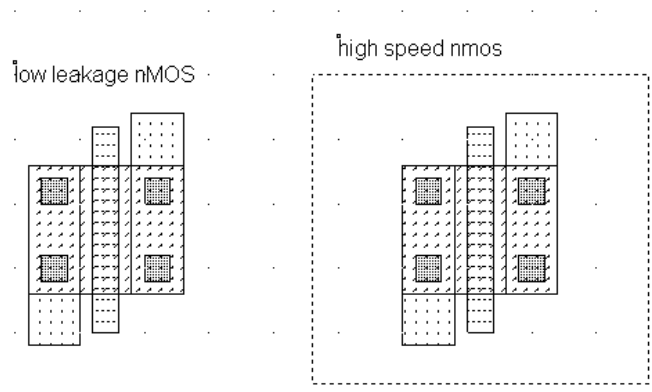


Figure 7: Layout of the low-leakage and high-speed MOS devices (*Mos/allMosDevices.MSK*). Dimensions are identical (2 lambda length).

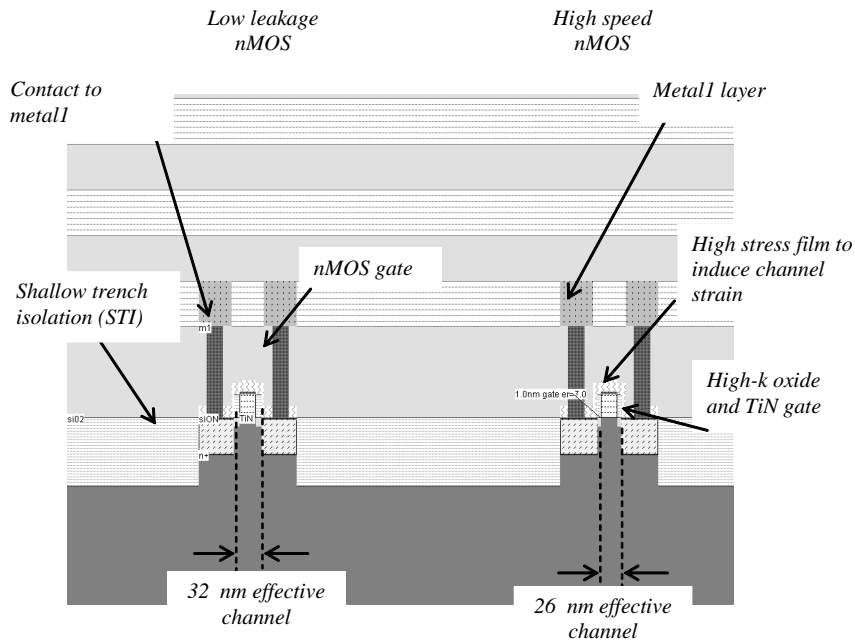


Figure 8: Cross-section of the nMOS devices (Mos/allMosDevices.MSK)

| Parameter | NMOS Low leakage | NMOS High speed |
|----------------------------|---------------------|--------------------|
| Drawn gate length (lambda) | 2 | 2 |
| Drawn gate length (nm) | 36 nm | 36 nm |
| Effective gate length (nm) | 32 nm | 26 nm |
| Threshold voltage (V) | 0.25 | 0.25 |
| Ion (mA/μm) at VDD=1.0V | 0.95 | 1.35 |
| Ioff (nA/μm) | 2 | 200 |

Table 3: nMOS parameters featured in the CMOS 32-nm technology provided in Microwind v3.5

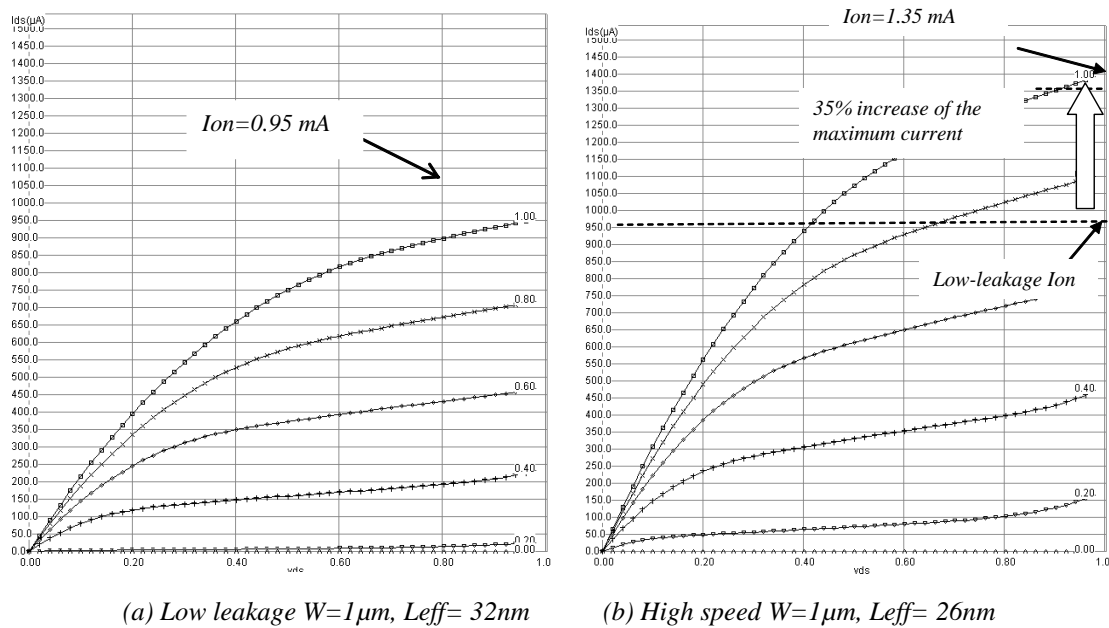


Figure 9: I_d/V_d characteristics of the low leakage and high speed nMOS devices. Note that $L_{\text{drawn}}=36\text{nm}$ in both cases. The effective length is significantly smaller for the high speed MOS

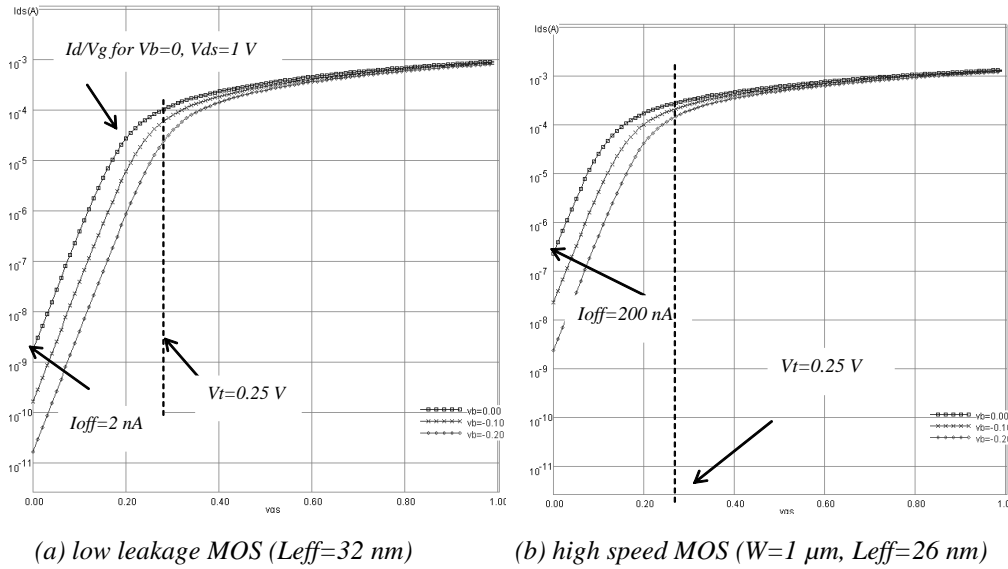


Figure 10: I_d/V_g characteristics (log scale) of the low leakage and high-speed nMOS devices

The I/V characteristics of the low-leakage and high-speed MOS devices (Figs. 9 and 10) are obtained using the MOS model BSIM4 (See [Sicard2007] for more information about this model). The I/V characteristics reported in Fig. 9 demonstrate that the low-leakage NMOS has a drive current capability of around 0.95 mA for $W=1.0 \mu\text{m}$ at a voltage supply of 1.0 V (0.95 mA/ μm). For the high speed NMOS, the effective channel length is slightly reduced (26 nm instead of 32 nm), to achieve a drive current around 1.35 mA/ μm .

The drawback associated with this high current drive is the leakage current which rises from 2 nA/ μm (low leakage NMOS) to 200 nA/ μm (high speed NMOS), as seen in the I_d/V_g curve at the X axis location corresponding to $V_g=0 \text{ V}$ (Fig. 10).

P-channel MOS device characteristics

The PMOS drive current in CMOS 32-nm technology (I_{on} in Table 4) is around 600 $\mu\text{A}/\mu\text{m}$ for the low-leakage MOS and up to 1000 $\mu\text{A}/\mu\text{m}$ for the high-speed MOS. The leakage current is around 1 nA/ μm for the low-leakage MOS and nearly 100 nA/ μm for the high-speed device.

| Parameter | pMOS Low leakage | pMOS High speed |
|---|---------------------|--------------------|
| Drawn gate length (lambda) | 2 | 2 |
| Drawn gate length (nm) | 36 | 36 |
| Effective gate length (nm) | 32 | 26 |
| Threshold Voltage (V) | -0.27 | -0.25 |
| I_{on} (mA/ μm) at VDD=1.0V | 0.60 | 1.00 |
| I_{off} (nA/ μm) | 1 | 100 |

Table 4: pMOS parameters featured by the 32-nm CMOS technology provided in Microwind v3.5

MOS Variability

One important challenge in nano-CMOS technology is process variability. The fabrication of millions of MOS devices at nano-scale induces a spreading in switching performances in the same IC. The most important parameters affected by process variability are the threshold voltage, the carrier mobility and the effective channel length. Variations are handled in Microwind using random values in a Gaussian distribution, which is expressed by the formulation of Equ. 2. An illustration of the variation in electron mobility (parameter U_0) for nearly a thousand MOS device samples is reported in Fig. 11.

$$f = \frac{1}{\sqrt{2\pi}\sigma} e^{-\frac{(x-m)^2}{2\sigma^2}} \quad (\text{Equ. 2})$$

where

f = probability density of the random variable (x axis in Fig. 11)

x = variable (y axis in Fig. 11)

σ = deviation

m = mean value

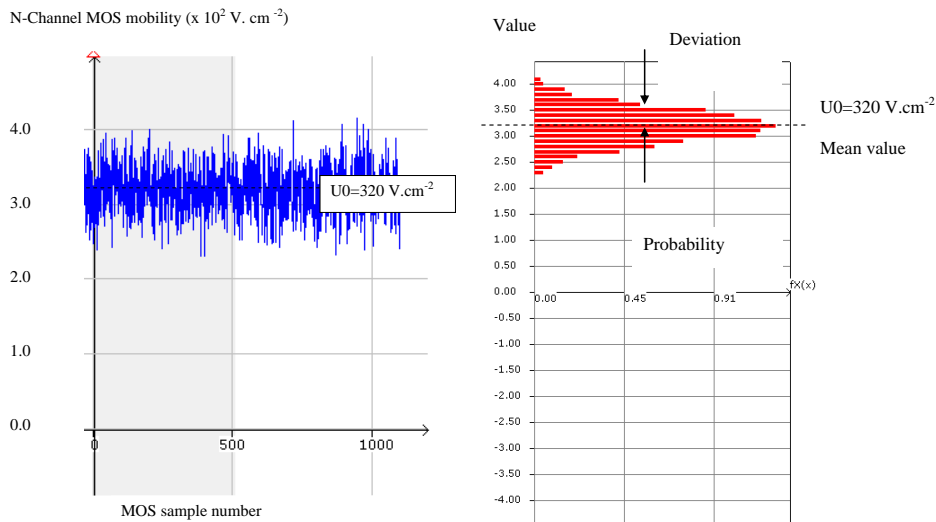


Figure 11: The extracted mobility of 1000 MOS samples shows an important variability around 320 V.cm⁻²

The effect of process variability on the MOS Ioff/Ion characteristics is plotted using the menu “Ioff vs. Ion” under the “MOS I/V curve” menu (Fig. 12). It can be seen that the MOS devices have a wide variability in performances. The 3 MOS types (low leakage, high speed, high voltage) are situated in well defined space in the Ioff/Ion domain. The low leakage is in the middle (medium Ion, low Ioff), the high speed on the upper right corner (high Ion, high Ioff), and the high voltage is at the lower left side of the graphics (low Ion, very low Ioff). Note that the exact locations of the dots will change for each MOS characteristics plotted because it is a random process.

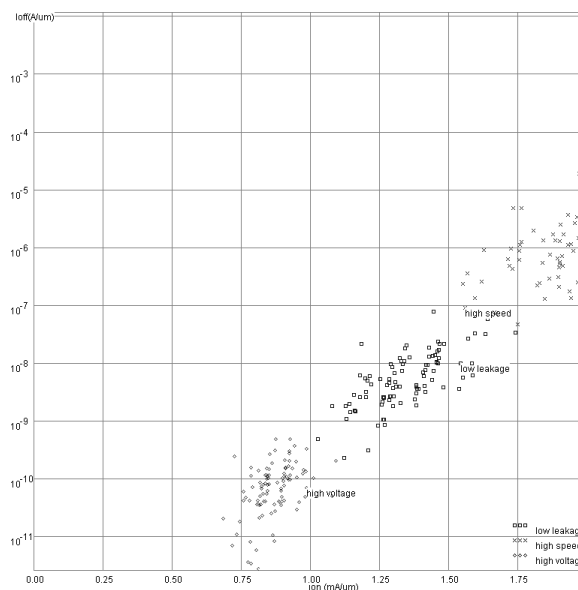


Figure 12: Ioff/Ion calculated by Microwind on 100 samples of n-channel MOS with random distribution of VT, U0, and LINT with a Gaussian distribution around the nominal value

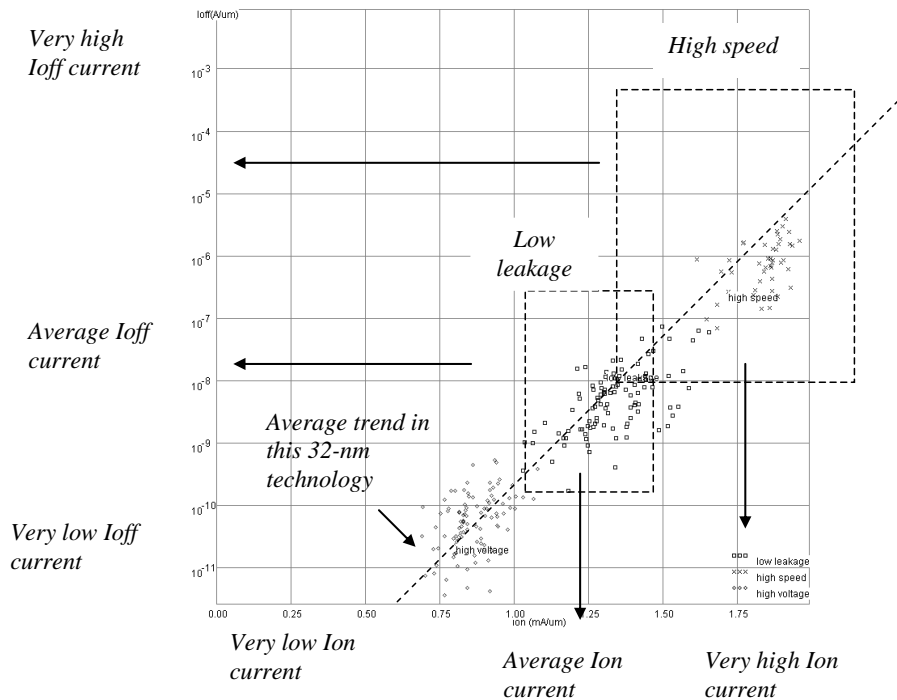


Figure 13: Finding compromises between high current drive and high leakage current

Concerning “worst case” and “best case”, notice that

- Slow devices have high V_T , low mobility U_0 and long channel ($LINT > 0$)
- Fast devices have low V_T , high mobility U_0 , and short channel ($LINT < 0$)

3. Interconnects

Metal Layers

As seen in the palette (Fig. 14), the available metal layers in 32-nm technology range from *metal1* to *metal8*. The layer *metal1* is situated at the lowest altitude, close to the active device, while *metal8* is nearly 5 μm above the silicon surface. Metal layers are labeled according to the order in which they are fabricated, i.e. from the lower level (*metal1*) to the upper level (*metal8*).

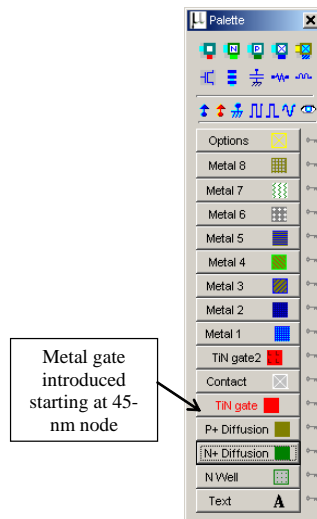


Figure 14: Microwind window with the palette of layers including 8 levels of metallization

In Microwind, specific macros are accessible to ease the addition of contacts in the layout. These macros can be found in the palette. As an example, you may instantiate a design-error free *metal7/metal8* contact by selecting *metal8*, followed by a click on the upper right corner icon in the palette. A *metal7/metal8* contact is depicted in Fig. 15. Additionally, access to complex stacked contacts is possible via the icon "complex contacts" situated in the palette, in the second column of the second row. The screen shown in Fig. 16 appears when you click on this icon. By default it creates a contact from poly to *metal1*, and from *metal1* to *metal2*. Tick more boxes "between metals" to build more complex stacked contacts.

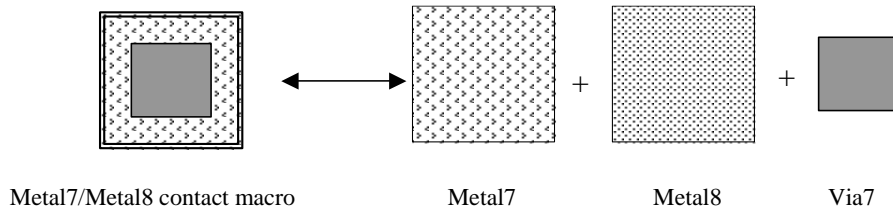


Figure 15: Access to contact macros between metal layers

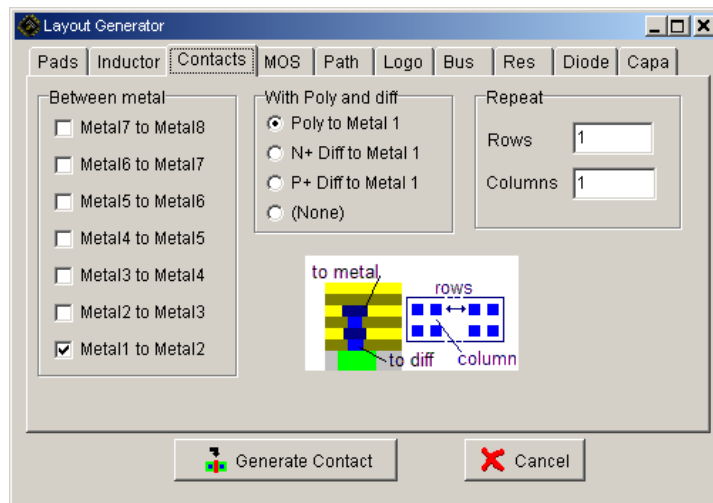


Figure 16: Access to complex contact generator

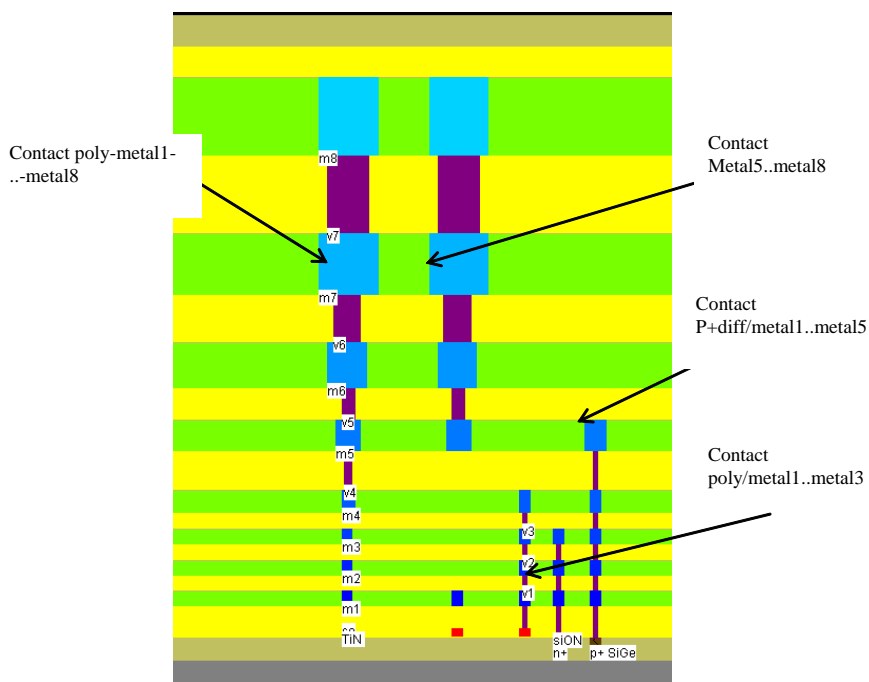


Figure 17: Examples of layer connection using the complex contact command from Microwind (Interconnects /Contacts.MSK)

Each metal layer is embedded into a low dielectric oxide (referred to as “interconnect layer permittivity K” in Table 2), which isolates the layers from each other. A cross-section of a 32-nm CMOS technology is shown in Fig. 17. In 32-nm technology, the layers *metal1..metal4* have almost identical characteristics. Concerning the design rules, the minimum width w of the interconnect is 3λ ($3 \times 18 \text{ nm} = 54 \text{ nm}$) and the minimum spacing is 4λ ($4 \times 18 \text{ nm} = 72 \text{ nm}$). The metal pitch is 7λ , that is 126 nm. Intel 32-nm CMOS technology specifies a similar value (112 nm) [Natarajan2008], while IBM specifies 100 nm pitch for metal 1 and 200 nm for metal 2.

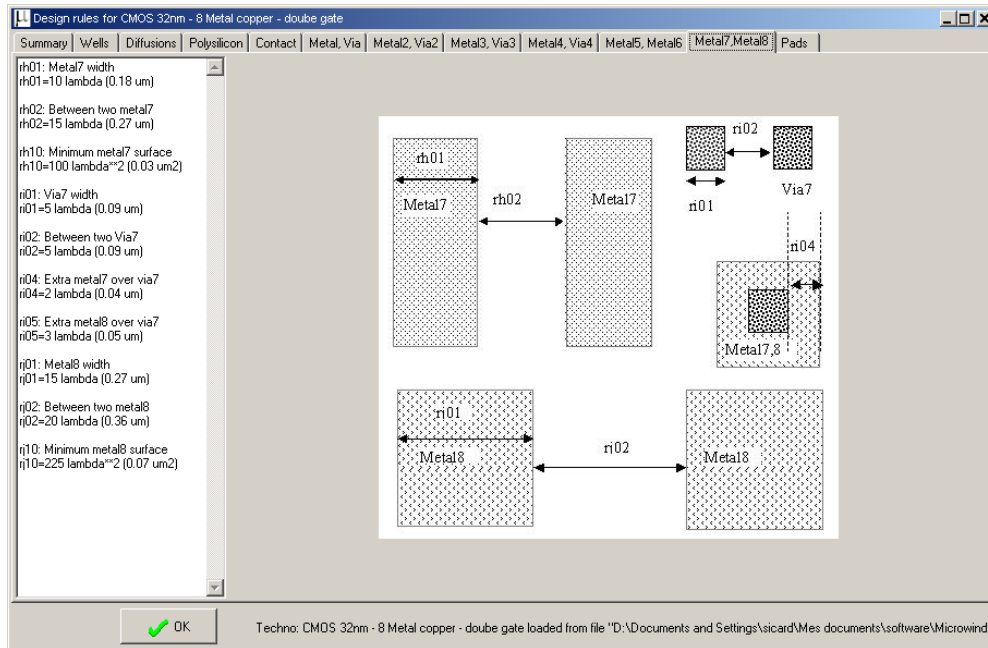


Figure 18: The Help > Design Rules menu of Microwind 3.5 gives details of the most important design rules

Layers *metal5* and *metal6* are a little thicker and wider, while layers *metal7* and *metal8* are significantly thicker and wider, to drive high currents for power supplies. The design rules for *metal8* are 15λ ($0.27 \mu\text{m}$) width, 20λ ($0.36 \mu\text{m}$) spacing (See Help > Design Rules, Fig. 18).

Interconnect Resistance

At minimum width ($3 \lambda \times 18 \text{ nm} = 54 \text{ nm}$), the interconnect resistance of the lower metal layers is around $7 \Omega/\mu\text{m}$ (Fig. 19), close to the value announced by Intel for metal 2 (8Ω) [Natarajan2008]. Metal layers 1 to 3 have the same dimensions and design rules, and consequently the same resistance.

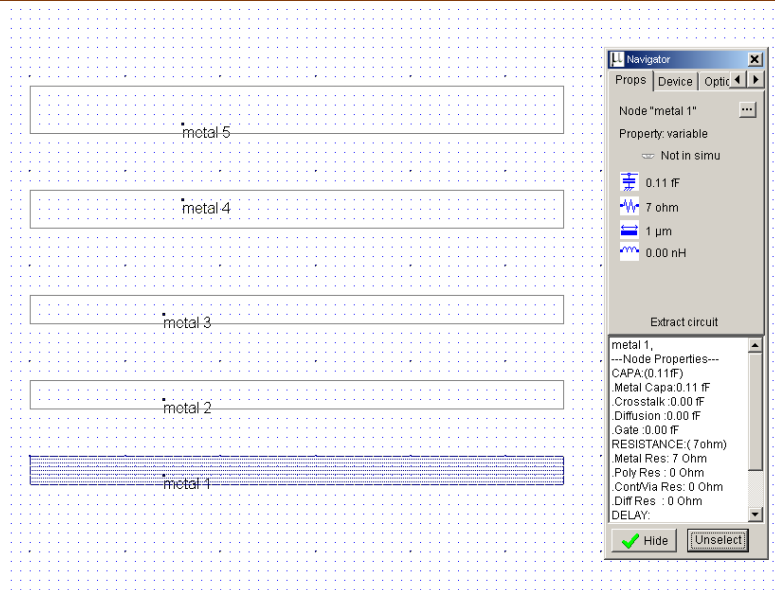
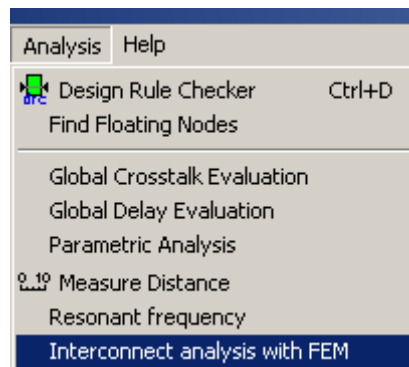


Figure 19: Computing the wire resistance (Interconnects > metal1-5.MSK)



Note that the resistance computed in Microwind from 2D values gives a smaller value for lower metal layers than that mentioned above. Click **Analysis** → **Interconnect Analysis with FEM**. For metal 1 up to metal 3, a value of $3.4 \Omega/\mu\text{m}$ is obtained, assuming entirely copper interconnect (Fig. 20). The reason for getting a higher resistance in practice is that the real conductor is a combination of copper and higher-resistivity material mandatory for the interconnect process, which almost doubles the resistance (Fig. 21).

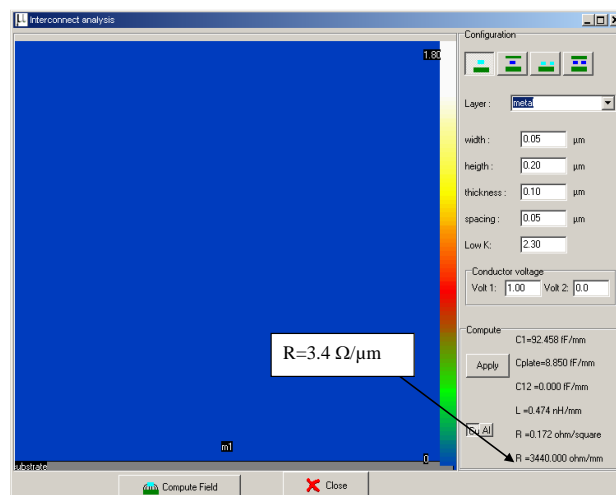


Figure 20: Extraction analysis of the wire resistance using “Interconnect Analysis with FEM”

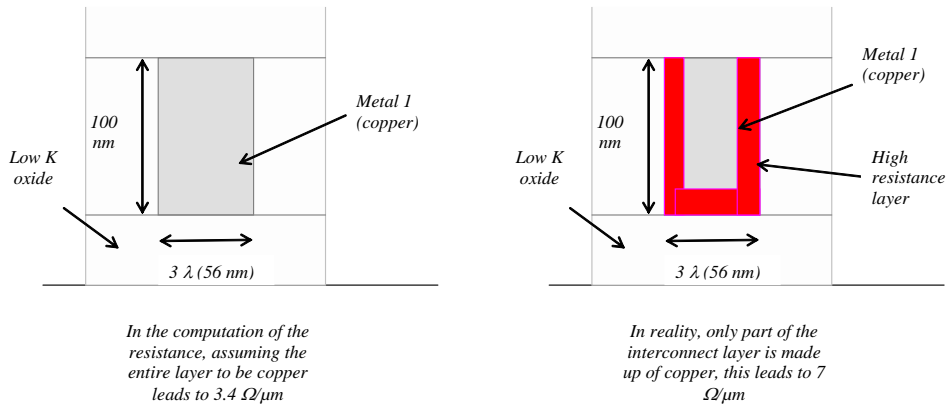


Figure 21: In reality, the lower metal layers feature a higher resistance, because the entire layer is not made up of low-resistivity material

Interconnect Capacitance

An average value of 0.2 fF/μm is found in the literature for metal 2 capacitance. Some details are given by Intel [Natarajan2008]. The usual setup consists of routing the lower and upper metal layers (resp. metal 1 and metal 3) at minimum pitch, as shown in Fig. 22, which is close to a realistic case. Consequently, the metal2 capacitance is much higher compared to when it is routed alone without surrounding metal interconnects. Note that the crosstalk capacitance, i.e. the capacitance between adjacent wires, is also quite large at minimum pitch.

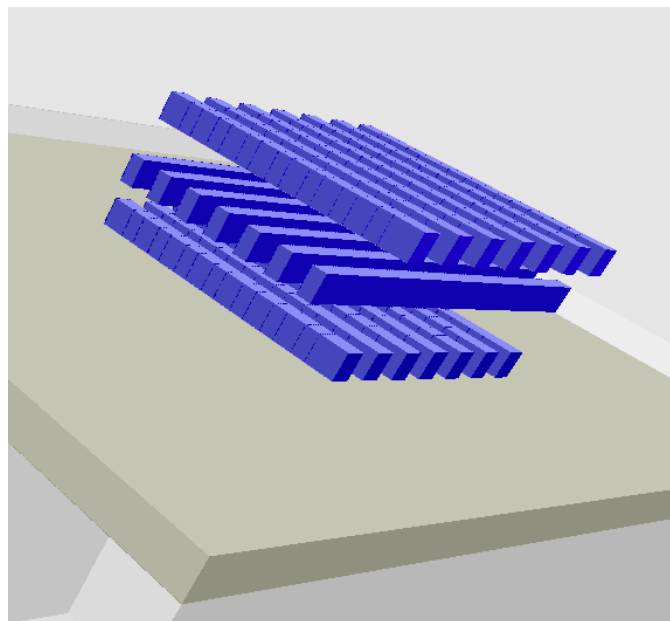


Figure 22: The interconnect capacitance is evaluated assuming that multiple wires are running below and above the layer under consideration (Interconnects > Metal1-3.MSK)

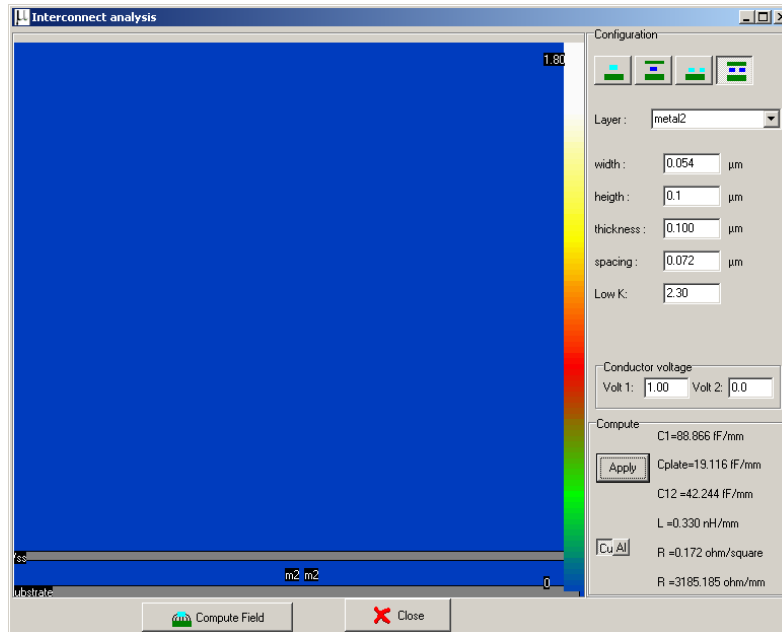


Figure 23: Realistic setup for evaluating metal2 total capacitance

The tool **Analysis** → **Interconnect analysis with FEM** may be used to evaluate the capacitance of such an interconnect. We select “metal 2” and the icon “Two conductors between 2 ground planes” situated at the upper right corner of the window. The default distance to ground (height) is 0.4μm, which corresponds to the distance from substrate to metal2. In the situation illustrated in Fig. 23, the distance between metal1 (considered as ground) and metal2 is much smaller: 0.1 μm. Consequently, we modify the height to 0.1μm and find C1=89 fF/mm and C12=42 fF/mm. As the setup considers one capacitance to ground and 2 possible crosstalk, the total capacitance is 0.173 fF/μm, close to the values measured by Intel:

$$C_{tot} = C_1 + 2.C_{12} \approx 173 \text{ fF/mm} = 0.173 \text{ fF/}\mu\text{m} \quad (\text{Equ. 3})$$

4. Designing in 32 nm technology

Ring Inverter Simulation

The ring oscillator made from 5 inverters, as shown in Fig. 24 (INV5.MSK), has the property of oscillating naturally. It can be simulated at layout level in Microwind using various technologies. We shall observe the oscillating outputs of the circuit for various technologies and measure their corresponding frequencies. The time period and frequency of the output signal are displayed in the Analog Simulation window (Fig. 25) if the “Frequency” box is selected. When running simulation you may observe the frequency of oscillation to be initially lower, increasing gradually with time and settling to the stable values reported above. Therefore it is important to run the simulations for long enough so that the correct (stable) oscillating frequency can be observed.

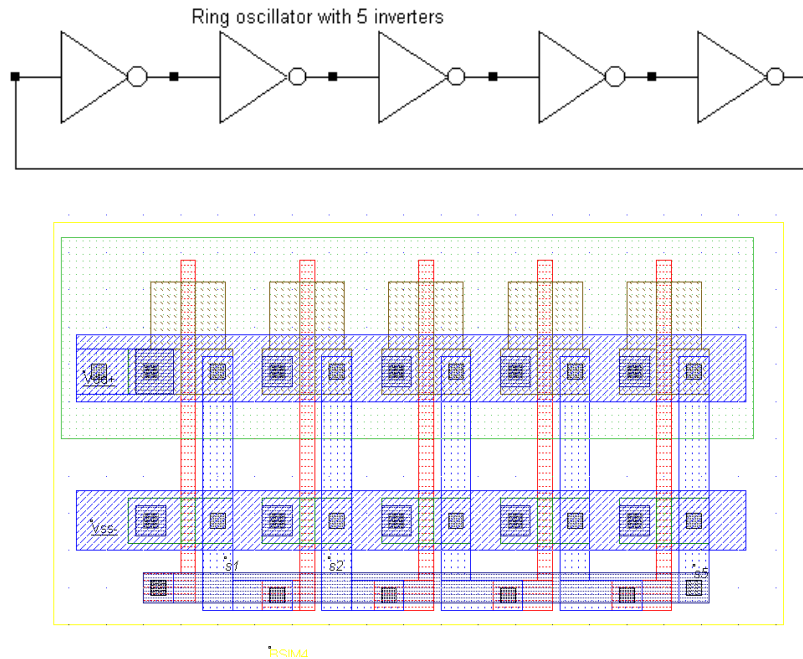


Figure 24: Schematic diagram and layout of the ring oscillator used for simulation (INV5.MSK)

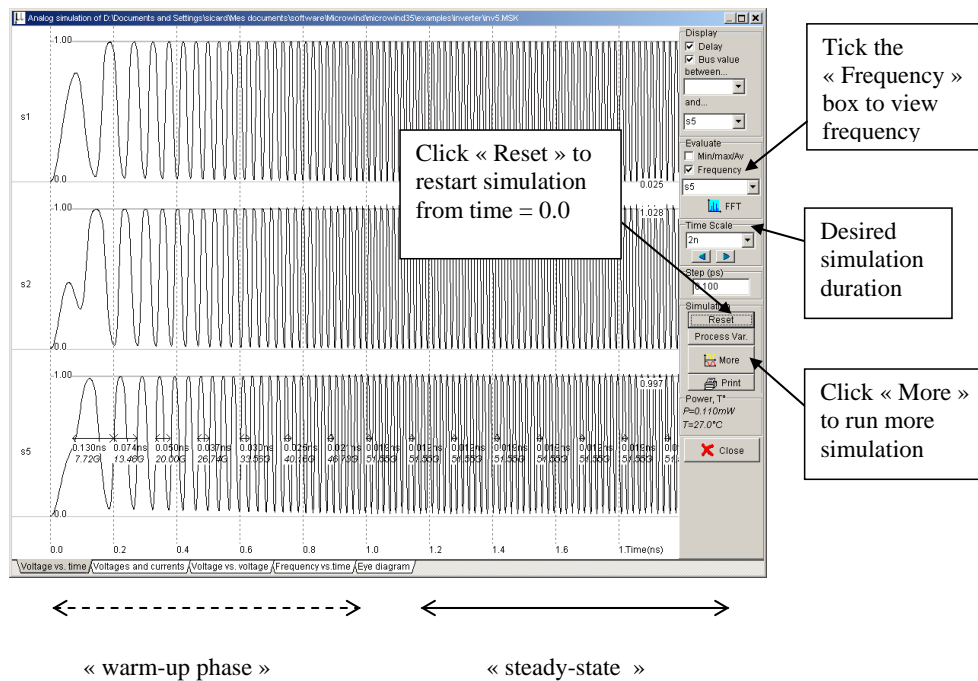


Figure 25: The simulation always starts by a “warm-up” phase (1.0 ns). Click “More” to run more simulation (Inverter > INV5.MSK)

| Technol ogy | Su ppl y | Oscillati on | Chronograms |
|----------------|----------------|-----------------|-------------|
| 0.8 μm | 5 V | 0.76GH z | |

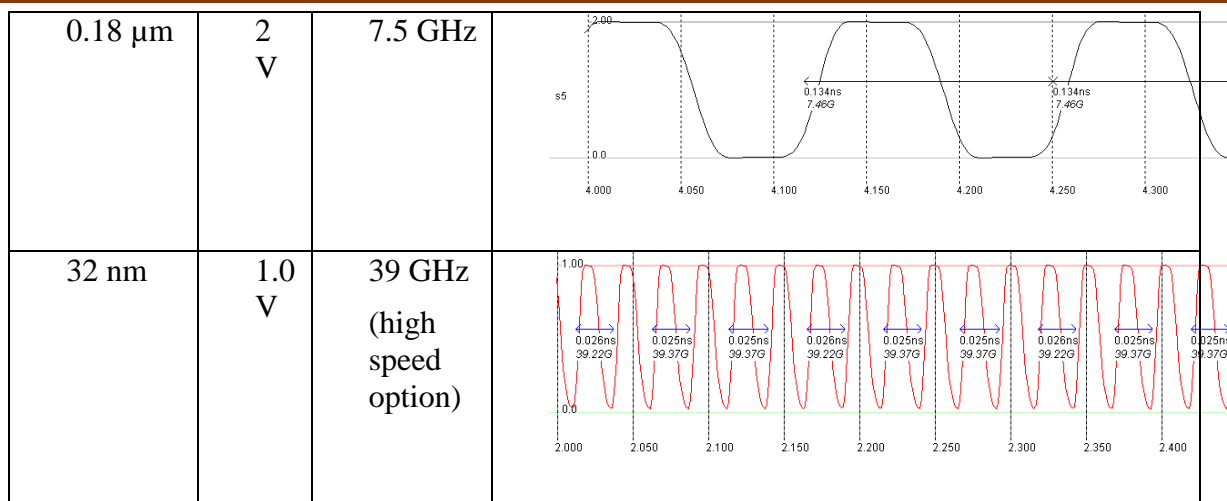


Figure 26: Oscillation frequency improvement with the technology scale down (Inv5.MSK)

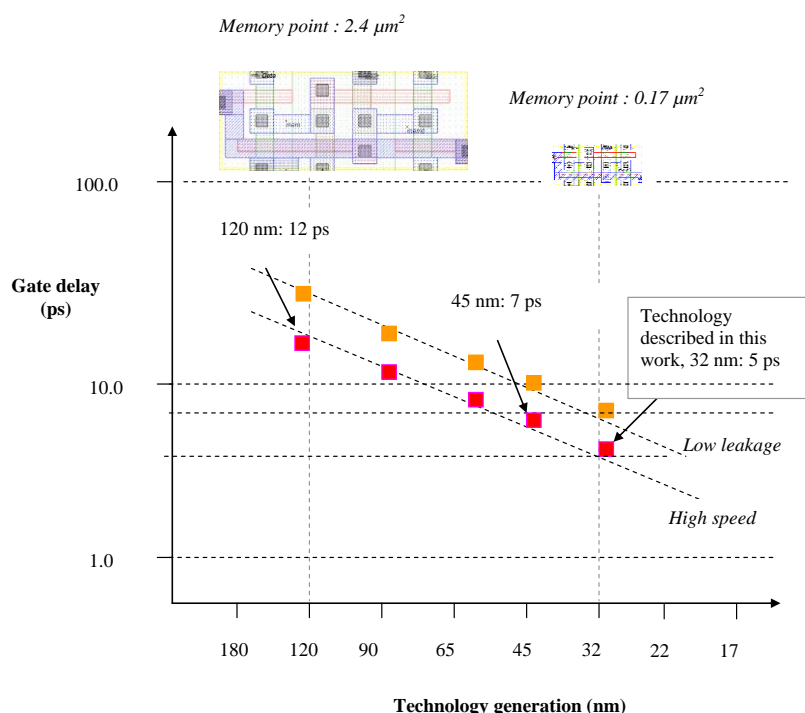


Figure 27: Comparison of gate delay for various technologies used in Microwind

The desired simulation duration can be selected from the drop down menu that appears under the “Time Scale” menu of the Simulation window. Remember to click the “Reset” button under the “Simulation” menu so that simulation results are refreshed for the selected duration. The time-domain waveforms of the outputs of the ring oscillator of Fig. 24 are reported in Fig. 26 for 0.8 μm , 0.18 μm and 32-nm technologies (high-speed option). Although the supply voltage (VDD) has been reduced (VDD is 5V in 0.8 μm , 2V in 0.18 μm , and 1.0 V in 32-nm), the gain in frequency improvement is significant.

Use the command **File** → **Select Foundry** to change the configuring technology. Sequentially select the **cmos08.RUL** rule file which corresponds to the CMOS 0.8- μm technology, then **cmos018.RUL** rule file (0.18 μm technology), and eventually **cmos32nm.RUL** which configures Microwind to the CMOS 32-nm technology. When you run the simulation, observe the change of VDD and the significant change in oscillating frequency (Fig. 26).

In Fig. 27, we plot the gate delay per stage for various technologies, as computed using Microwind on a 5-inverter ring oscillator. We divide the one-cycle delay by the number of stages

to obtain the gate delay plotted in Y axis. We can observe that the improvement in switching delay with technology scaling is significant although not impressive. Let us recall that the cell density has been improved by a factor of 10 between the 120 nm generation and the 32 nm generation.

High Speed vs. Low leakage

Let us consider the ring oscillator with an enable circuit, where one inverter has been replaced by a NAND gate to enable or disable oscillation (Inv5Enable.MSK). The schematic diagram of the oscillator and its layout implementation are shown in Fig. 28. We analyze its switching performance using high speed and low leakage MOS devices. The results are summarized in Fig. 28.

As shown in Fig. 29 the box "Scale I log" must be selected (ticked) to display the current in logarithmic scale. To select the "high speed" or "low leakage" MOS device **click** inside the *option layer box* in the layout which surrounds all the oscillator devices, and then select "high speed" or "low leakage" in the **Navigator** window. These actions are illustrated in Fig. 30. From the analog performances shown in Fig. 29~~28~~ we observe that the circuit works faster in the high speed mode (35 GHz) but consumes a significant amount of standby current, i.e. when it is off (around 100 nA).

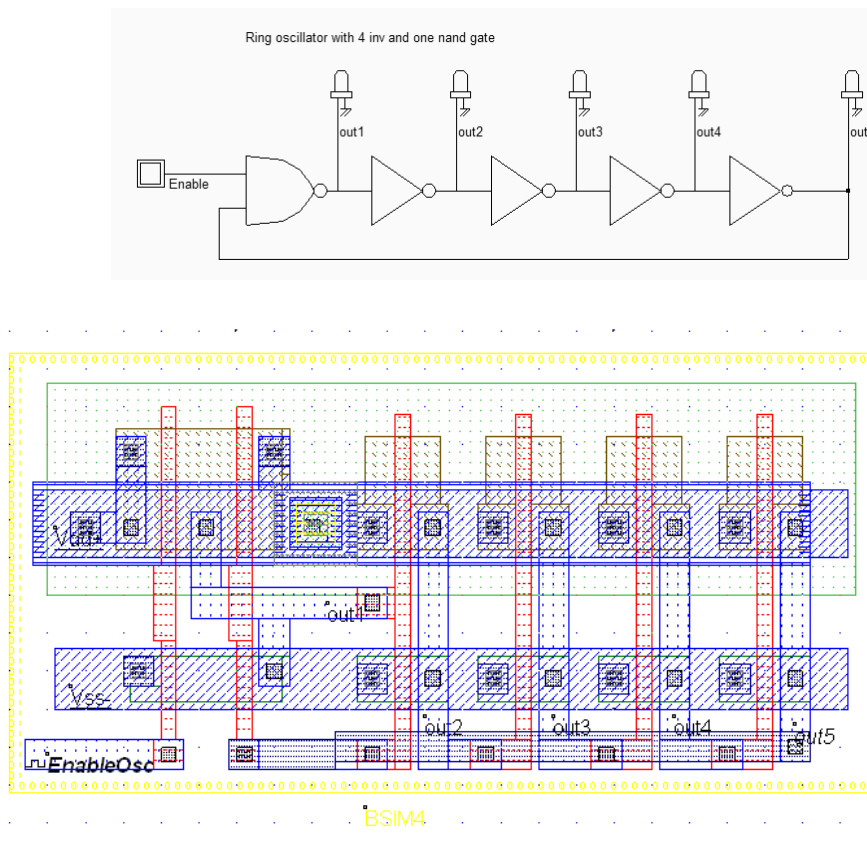


Figure 28: The schematic diagram and layout of the ring oscillator used to compare the analog performances in high speed and low leakage modes (INV5Enable.MSK)

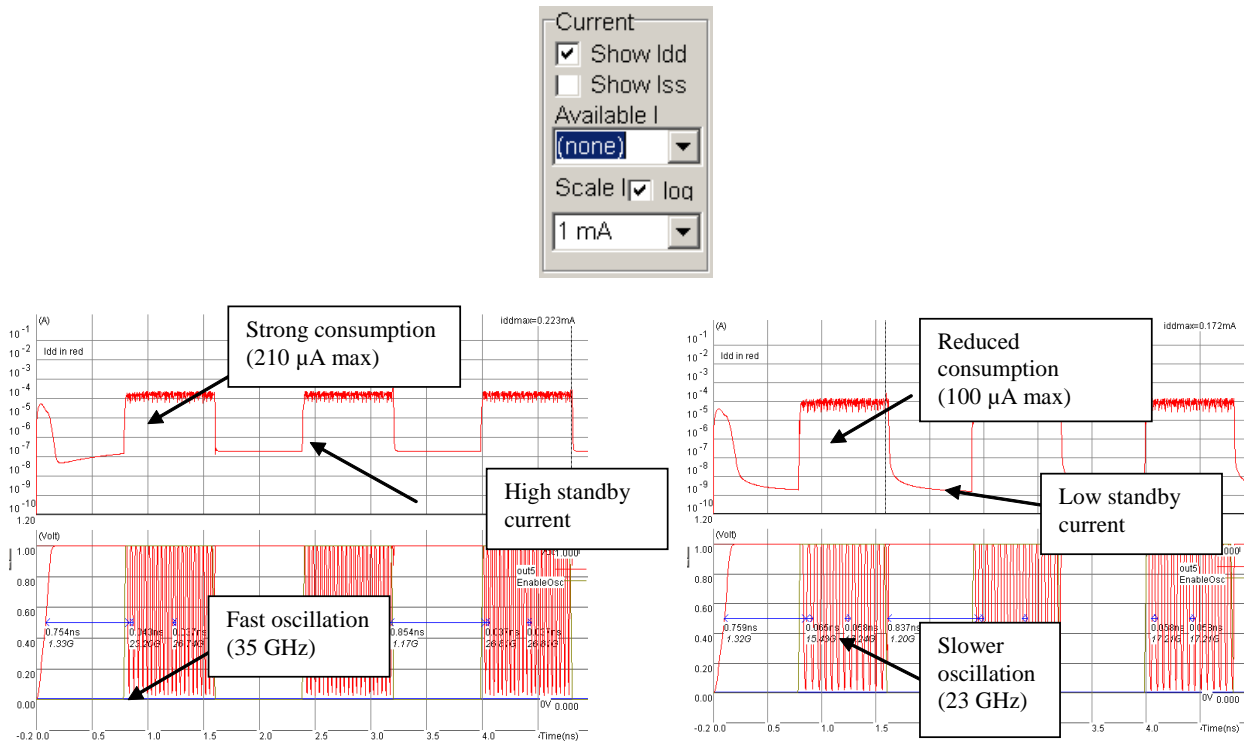


Figure 29: Simulation of the ring oscillator in high speed mode (left) and low leakage mode (right). The oscillating frequency is higher in high-speed mode but the standby current is also high (Inv5Enable.MSK)

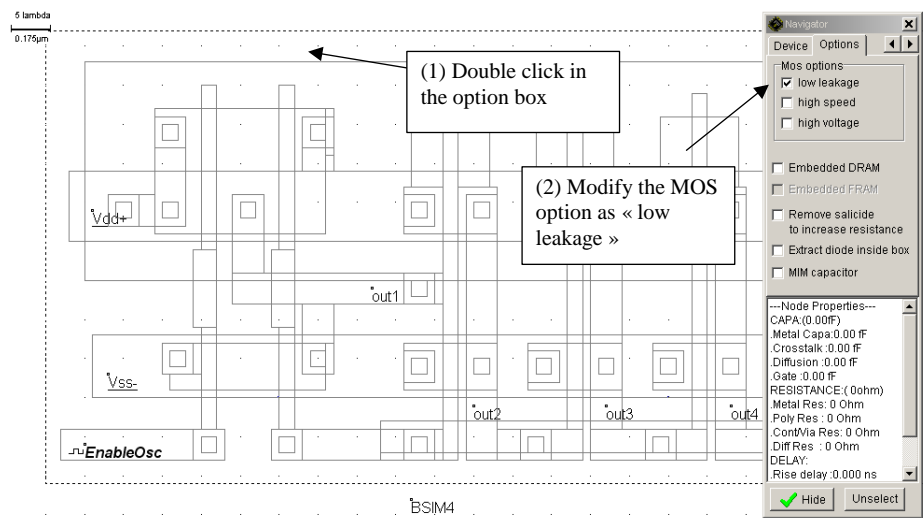


Figure 30: Changing the MOS option into low leakage mode

The low-leakage mode features a little slower oscillation (23 GHz, that is approximately a 40% speed reduction) and nearly 2 decades less standby current (several nA after a delay). In summary, low leakage MOS devices should be used as default devices whenever possible. High speed MOS devices should be used only when switching speed is critical.

Simulation of Process Variations (PVT)



Microwind 3.5 gives access to “Process-Voltage-Temperature” (PVT) simulation through the command **Simulate** → **Simulation Parameters** → **Process Variations**. Direct access from the simulation waveform window is also possible using the button “**Process Var.**”. The most usual simulation consists of simulating extreme situations (Min and Max), as compared to typical conditions, as shown in Fig. 31. The parametric variations are summarized in Table 5. In Fig. 31, nearly 100% variation is observed between the performances under Min and Max situations.

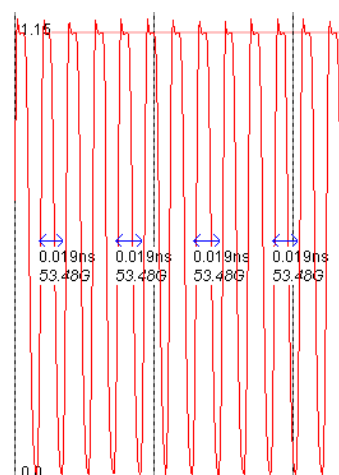
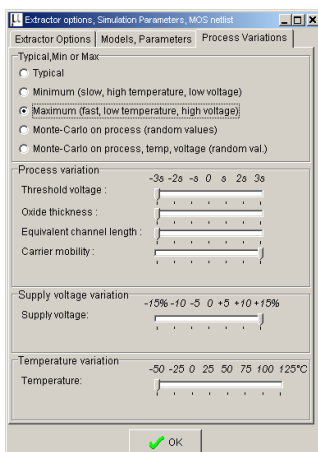
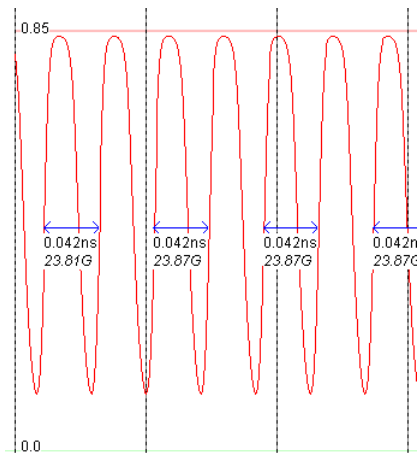
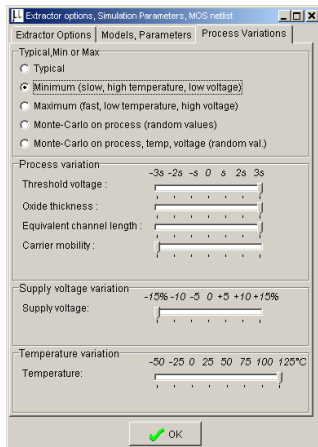


Figure 31: PVT Min-Max simulation showing 100% variation in switching performances

Notice that

- In Min situation, V_T is high, mobility U_0 is low and the channel is long ($LINT > 0$). The supply is minimum and the temperature is maximum.
- In Max situation, V_T is low, mobility U_0 is high and the channel is short ($LINT < 0$). The supply is maximum and the temperature is minimum.

| Parameter class | Parameter | Symbol (BSIM4) | Unit | Min (32-nm) | Typ (32-nm) | Max (32-nm) |
|-----------------|--------------------------|----------------|--------------------|-------------|-------------|-------------|
| Process | Threshold Voltage | V_T | V | 0.30 | 0.25 | 0.20 |
| | Mobility | U_0 | cm.V^{-2} | 500 | 600 | 700 |
| | Channel length reduction | LINT | m | $2e^{-9}$ | 0 | $-2e^{-9}$ |
| Voltage | Supply | VDD | V | 0.85 | 1.0 | 1.15 |
| Temperature | Temperature | TEMP | $^{\circ}\text{C}$ | 125 | 27 | -50 |

Table 5: Variation of process parameters

6-transistor static RAM

One of the most representative designs for comparing technology nodes is the static RAM cell designed using 6 transistors (6T-SRAM). In our implementation in Microwind (see Fig. 32), the layout size is $0.28 \times 0.66 \mu\text{m}$, with a surface area of $0.19 \mu\text{m}^2$, which a little larger than the published data (Intel: $0.16 \mu\text{m}^2$, IBM $0.17 \mu\text{m}^2$). Note that the layout strictly obeys the basic design rules. Most contacts are shared with neighboring cells: the VSS, VDD contacts, the Select and Data lines. It is usual to find more aggressive layout design rules in RAM cell designs, in order to further decrease the cell area.

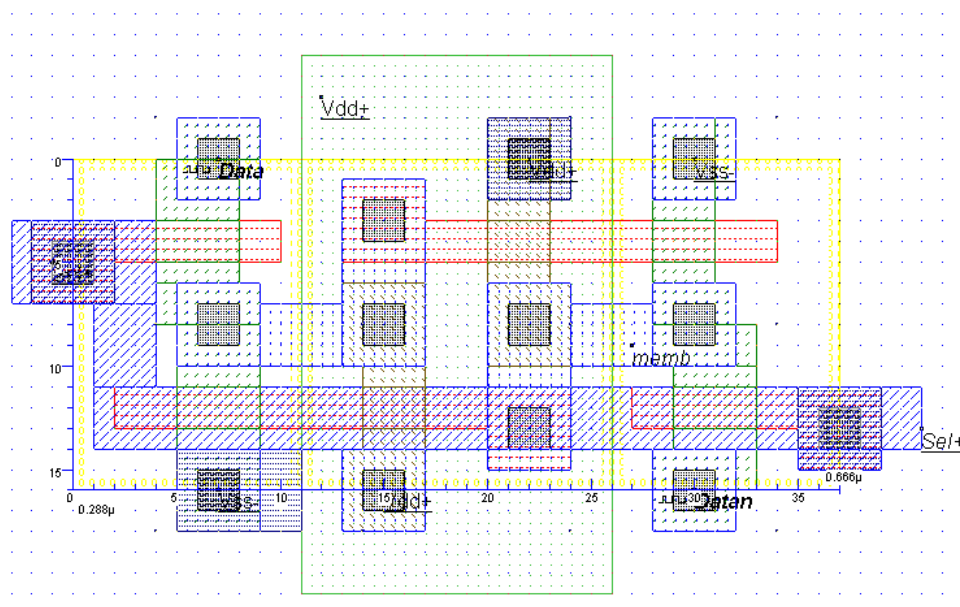


Figure 32: The 6-transistor RAM layout using 32-nm design rules (Ram6T_32nm.MSK)

5. Conclusions

This application note has illustrated the trends in CMOS technology and introduced the 32-nm technology generation, based on technology information available from integrated circuit manufacturers. A set of specific topics has been addressed, including the new gate dielectric, gate stack and the strained silicon technique for enhanced mobility, the 8-metal interconnect back-end process and the 32-nm process variants. N-channel and P-channel MOS device characteristics have been presented, as well as a comparative study of a ring inverter oscillator for various technology nodes. Finally, performance of the ring oscillator in the high speed and low leakage modes have been compared, with the impact on speed and leakage current. Future work will concern the 22-nm technology node, under preparation for an industrial production in 2012.

References

- [Arnaud2008] F. Arnaud et al, “32nm General Purpose Bulk CMOS Technology for High Performance Applications at Low Voltage”, *IEDM Tech Dig.*, 2008, pp. 1-4.
- [Chen2008] C X. Chen et al, “A Cost Effective 32nm High-K/ Metal Gate CMOS Technology for Low Power Applications with Single-Metal/Gate-First Process”, *Symposium on VLSI Technology Digest of Technical Papers*, 2008, pp. 88-89.
- [Common2009] The Common Platform technology model is focused on 90-nm down to 32-nm technology <http://www.commonplatform.com>
- [Diaz2008] C. H. Diaz et al, “32nm Gate-First High-k/Metal-Gate Technology for High Performance Low Power Applications”, *IEDM Tech Dig.*, 2008, pp. 1-4.
- [Hasegawa2008] S. Hasegawa et al, “A Cost-Conscious 32nm CMOS Platform Technology with Advanced Single Exposure Lithography and Gate-First Metal Gate/High-K Process”, *IEDM Tech Dig.*, 2008, pp. 1-3.
- [ITRS2009] The ITRS roadmap for semiconductors may be downloaded from <http://www.itrs.net>
- [Natarajan2008] S. Natarajan et al, “A 32nm Logic Technology Featuring 2nd-Generation High-k + Metal-Gate Transistors, Enhanced Channel Strain and 0.171 μ m² SRAM Cell Size in a 291Mb Array”, *IEDM Tech Dig.*, 2008, pp. 1-3.
- [Sicard2006] E. Sicard and S. M. Aziz, “Introducing 65-nm technology in Microwind3”, software application note, July 2006, www.microwind.org
- [Sicard2007] E. Sicard, S. Ben Dhia “Basic CMOS cell design”, McGraw Hill, 450 pages, international edition 2007 – ISBN 9780071488396
- [Sicard2008] E. Sicard and S. M. Aziz, “Introducing 45-nm technology in Microwind3”, software application note, July 2008, www.microwind.org
- [Sicard2009] E. Sicard “Microwind User’s Manual, lite version 3.5”, INSA editor, 2009, www.microwind.org.
- [Skotnicki2008] Skotnicki, T. and all, “Innovative Materials, Devices, and CMOS Technologies for Low-Power Mobile Multimedia”, *IEEE Trans. Electron Device*, Vol 55, N°1, pp 96-130